Macromolecular Journals

Macromolecular Chemistry and Physics

Trends in Polymer Science

What Morphologies Do We Want? – TEM Images from Dilute Diblock Copolymer Solutions

Hong Zhao, Qianjin Chen, Liangzhi Hong, Lei Zhao, Jianfang Wang,* Chi Wu*

The formation of various exotic morphologies of block copolymers in dilute solutions has often been claimed on the basis of TEM imaging. Do they really exist in solutions or are they just some kinetically frozen structures arising from TEM sample preparation? It is shown that different morphologies are formed due to a competition between different time scales. More and more people are realizing that it is necessary to use cryo-TEM to ascertain a novel morphology in polymer solutions, but not everyone is able to access a modern cryo-TEM. Our current study serves as an alarm to those who are interested in morphologies in block copolymer solutions that it is necessary to combine different methods, such as LLS, freeze-drying, and TEM, in their studies.

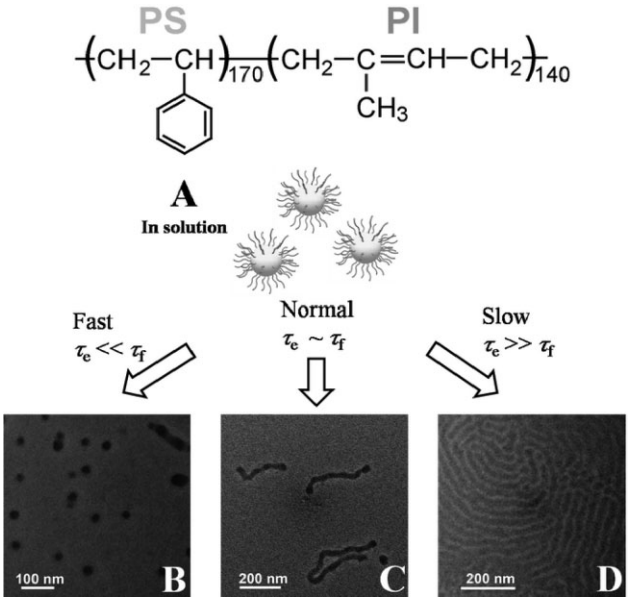

H. Zhao, Q. Chen, L. Hong, C. Wu
Department of Chemistry, The Chinese University of Hong Kong, Shatin, Hong Kong
E-mail: chiwu@cuhk.edu.hk
C. Wu
Department of Chemical Physics, The Hefei National Laboratory of Physical Sciences at Microscale, University of Science and Technology of China, Hefei, Anhui 230026, China
L. Zhao, J. Wang
Department of Physics, The Chinese University of Hong Kong, Shatin, Hong Kong
E-mail: jfwang@phy.cuhk.edu.hk

Introduction

The formation of block copolymer micelles with different morphologies has fascinated polymer researchers for more than two decades. There is no any slow-down sign in this still-booming field termed by some eyes-catching words like "self-assembly," "supramolecules," "nanoscience" or "nanotechnology," to name but a few. It is indeed important to study "disorder-to-order" and "order-to-order" phase transition in systems made of block copolymers, especially in melts and blends, and relate them to various interactions among polymer chains, different blocks, and solvent molecules. These block copolymer systems also have some potential applications such as drug carrier for cancer therapy,[1,2] templates to align metal and semiconductor nano-crystals into one-dimensional arrays.[3,4]

Various morphologies of block copolymer micelles in films and bulk have been widely studied.[5–9] The micelle formation is basically governed by

DOI: 10.1002/macp.201000696

the interaction among different blocks. In solutions, a selective solvent is often used to fine turn the association of the insoluble blocks, which involves the interactions between the solvent and different blocks; namely, the solubility difference. For neutral block copolymers in organic solvents, besides the loss of some translational and conformational entropies, the micelle morphology is mainly governed by a force balance among the core block attraction, the corona block repulsion, and the core-corona interfacial tension.[10] In general, such a force balance can be adjusted by tuning the copolymer molecular structure,[11,12] block composition,[13,14] copolymer concentration,[15] solvent composition,[8,16,17] and temperature.[18,19] There have already been some systematic studies on the morphological transitions of copolymer micelles among spheres, cylinders, and vesicles. The transition kinetics has also been found to depend on how the micelles are initially prepared.[20] The Bates group[21] observed a sequence of shapes from vesicles through cylinders to spheres of polybutadiene-*block*-poly(ethylene oxide) (PB-*b*-PEO) diblock copolymers in water by changing the composition of the hydrophilic PEO block. Eisenberg and his coworkers[13–16,22] investigated the morphologies of polystyrene-*block*-poly(acrylic acid) (PS-*b*-PAA) ionic diblock copolymers in solvent mixtures of water and dimethylformamide. On the other hand, some experiments have also been devoted to the exploration of micelle morphologies in organic solvents, where the transitions from spheres to cylinders are induced by controlling the solution temperature[18] or applying an external pressure.[23,24]

More and more people realize that new cryogenic transmission electron microscopy (cryo-TEM) is a powerful technique to freeze different morphologies of polymeric aggregate or surfactant micelles in dispersions.[6,8,21,25] However, not everyone is able to access a modern cryo-TEM, especially when organic solvents are used. Currently, many "novel" morphologies are still reported only based on TEM images without rigorous structural characterization in solutions. On the other hand, to our knowledge, there has been no systematic comparison between morphologies of polymeric micelles obtained in solutions by scattering methods and in cryo-TEM.

The micelle morphology also plays a role in block copolymer lithography, a promising potential approach for the fabrication of nano-scale materials and devices. It can lead to feature sizes down to 10–30 nm. External fields, such as electric[26,27] and magnetic fields,[28] shear,[29] and temperature gradients,[30] have been widely utilized to control the orientation and lateral ordering of the nano-scale domains in block copolymer films. Exposing copolymer films to good solvents could generate long-range equilibrium morphologies because of an increase in the chain mobility.[31] An in-depth understanding of the formation of equilibrium structures or kinetically trapped morphologies during solvent annealing requires not only a proper choice of solvents but also some judicious controls of experimental parameters, such as the vapor pressure, treatment time, and solvent extraction rate.

We previously measured the hydrodynamic force required to pull individual polystyrene-*b*-polyisoprene (PS-*b*-PI) chains out of each spherical micelle by forcing them through a 20-nm pore,[32] and further discovered that the addition of a proper amount of tetrahydrofuran (THF), a good solvent for both PI and PS, can lead to a transition from spherical micelles to metastable cylindrical ones when the solution was extruded through the pore during an ultra-filtration process.[23]

Further, we tried to characterize morphologies of PS-*b*-PI diblock copo-

Hong Zhao received the B.Sc. from the Xiamen University in 2008, specializing in life science. He is now pursuing Ph.D. studies in the Department of Chemistry at The Chinese University of Hong Kong under the supervision of Prof. Chi Wu. His current research work mainly focuses on obtaining the amyloid-like protein (Sup 35 and Huntington exon 1) in a unimer state and the initial stage of the amyloid-like protein aggregation process by using laser light scattering.

Jianfang Wang obtained his B.S. degree (1993) in chemistry and software design from the University of Science and Technology of China, his M.S. degree (1996) in chemistry from Peking University and his Ph.D. degree (2002) in physical chemistry from Harvard University. After being a postdoctoral researcher in the University of California, Santa Barbara from February 2002 to July 2005, he moved to The Chinese University of Hong Kong in August 2005 as an assistant professor in the Department of Physics. His current research interests are the synthesis and plasmonic properties of metal nanocrystals, and multifunctional nanostructured materials.

Chi Wu graduated from Chemical Physics at the University of Science and Technology of China (1982) and obtaining his Ph.D. (1987) at the State University of New York at Stony Brook under the supervision of Professor Benjamin Chu. After working at BASF (Ludwigshafen, Germany) from 1989–1992, he joined the Department of Chemistry at the Chinese University of Hong Kong as a Lecturer. In 1999, he became a Chair Professor of Chemistry and Honorary Professor of Physics. He combines synthetic chemistry, polymer physics, and molecular biology to design and execute decisive experiments to answer important questions in macromolecules, colloids, and biology.

lymer micelles in the solvent mixture with different hexane/THF ratios before the nanopore extrusion. Surprisingly, LLS studies showed the presence of only spherical swollen micelles when the THF content increases and a final dissolution of the micelles into individual chains. The laser light scattering (LLS) results are consistent with thermodynamic expectation. Namely, as the solvent quality becomes better for both PS and PI, a larger core-corona interfacial area can be stabilized by the PI blocks. However, TEM imaging showed an unexplainable morphological transition from spheres through cylinders to flower-like structures when the TEM samples were prepared under ambient air at the room temperature. Such contradictive results obtained from TEM and LLS have forced us to look into the effect of the solvent evaporation rate on the TEM sample preparation. Our results reveal that different morphologies are obtainable by controlling the evaporation rate. This leads to a question "what morphologies do we want?" Our essential message is that there is no correlation between micelle structures in solutions and morphologies observed in TEM based on dilute solution-casted thin films, especially without an annealing at temperatures higher than the glass transition temperature. Therefore, one has to be careful or cautious to claim a novel morphology only based on TEM results.

Experimental Part

Sample Preparation

The diblock copolymer PS_{170} -*b*-PI_{140} was synthesized by using high-vacuum living anionic polymerization, which was initiated by the use of *sec*-butyllithium in cyclohexane at 45 °C. The detailed synthetic procedure can be found in ref.[32] The resultant copolymer was characterized using size exclusion chromatography with a multi-angle LLS detector, a combination of static and dynamic LLS, and proton nuclear magnetic resonance. The copolymer has a narrow size distribution with a polydispersity index of 1.06.

The solutions were prepared by adding a calculated amount of the copolymer into an appropriate volume of THF. After a complete dissolution of the copolymer into individual chains in THF, a calculated amount of hexane was added dropwise under stirring. The final THF content in the binary solvent mixture was in the range 3–25 vol.-%. In addition, a solution of the copolymer in pure hexane was also prepared, i.e., 0 vol.-% THF. In this study, the copolymer concentration was kept at 5.0×10^{-4} g · mL^{-1}. Each resultant solution was remained at the room temperature for more than 2 months to ensure that it reached its thermodynamic equilibrium state before use. Both THF and hexane were filtrated with a 0.45 μm hydrophobic polytetrafluoroethylene (PTFE) membrane filter (Millipore) before the sample preparation.

Laser Light Scattering

A commercial LLS spectrometer (ALV/DLS/SLS-5022F) equipped with a multi-τ digital time correlator (ALV5000) and a cylindrical 22 mW He-Ne laser (632.8 nm, Uniphase) as the light source was utilized to characterize the obtained copolymer micelles. Dust particles were removed by a filtration of each copolymer solution through a 0.45 μm PTFE membrane. All of the LLS experiments were performed at 25 °C. In static LLS, the weight-average molar mass, $\overline{M}_w$, and the z-average root-mean-square radius of gyration, $\langle R_g^2 \rangle^{1/2}$, of polymer micelles in dilute solutions can be determined from the angular dependence of the excess absolute scattering intensity, known as the Rayleigh ratio $R_{vv}(q)$, according to

$$\frac{KC}{R_{vv}(q)} \approx \frac{1}{\overline{M}_w}\left(1 + \frac{1}{3}\langle R_g^2 \rangle q^2\right) + 2A_2C \quad (1)$$

where $K = 4\pi^2 n^2 (dn/dC)^2/(N_A \lambda_0^4)$, and $q = (4\pi n/\lambda_0)\sin(\theta/2)$ with N_A, n, θ, and λ_0 being the Avogadro number, the solution refractive index, the scattering angle, and the wavelength of the laser light in vacuum, respectively; C is the polymer concentration; and A_2 is the second virial coefficient.

In dynamic LLS, the Laplace inversion of each measured intensity-intensity time correlation function $G^{(2)}(t,q)$ in the self-beating mode gives a line-width distribution function $G(\Gamma)$. For a pure diffusive relaxation, Γ is related to the translational diffusion coefficient D by $\Gamma = Dq^2$ when $q \to 0$ and $C \to 0$. D is further related to the hydrodynamic radius R_h by the Stokes-Einstein equation, $R_h = k_B T/6\pi\eta D$, where k_B, T, and η are the Boltzmann constant, the absolute temperature, and the solvent viscosity, respectively.

TEM Imaging

The TEM imaging was performed on an FEI CM120 microscope operated at 120 kV. The TEM samples were prepared in three ways. They are named as the fast, normal, and slow evaporation. For the fast evaporation, the samples were prepared by placing 10 μL drops of the copolymer solutions onto carbon-coated copper grids, followed by drying in ambient air with a hair dryer. For the normal evaporation, the copolymer solution droplets deposited on copper grids were dried naturally in air at room temperature. For the slow evaporation, a glass beaker was first filled with the binary solvent mixture that was used to make the copolymer solution. A solid support was placed in the beaker, with the top of the support kept above the surface of the liquid solvent. A copper grid was then transferred onto the support in the beaker. The beaker was hermetically covered and kept still for 30 min to let the top part of the beaker filled with the saturated vapor. A 10 μL drop of the copolymer solution was then placed onto the copper grid through a syringe, followed by drying in the solvent vapor overnight. Under the fast, normal, and slow evaporation conditions, the solution droplets on the copper grids were seen to disappear after a few seconds, ≈3 min, and ≈30 min, respectively. The as-prepared samples on copper grids were kept in a desiccator for 1–3 d before the TEM imaging.

Results and Discussion

Figure 1 shows that as the THF content increases from 0 to 19 vol.-%, the morphology has gradually developed from spherical to cigar-shaped micelles, then to worm-like cylindrical micelles, and finally to an exotic flower-like structures made of twisted long cylindrical micelles, where these

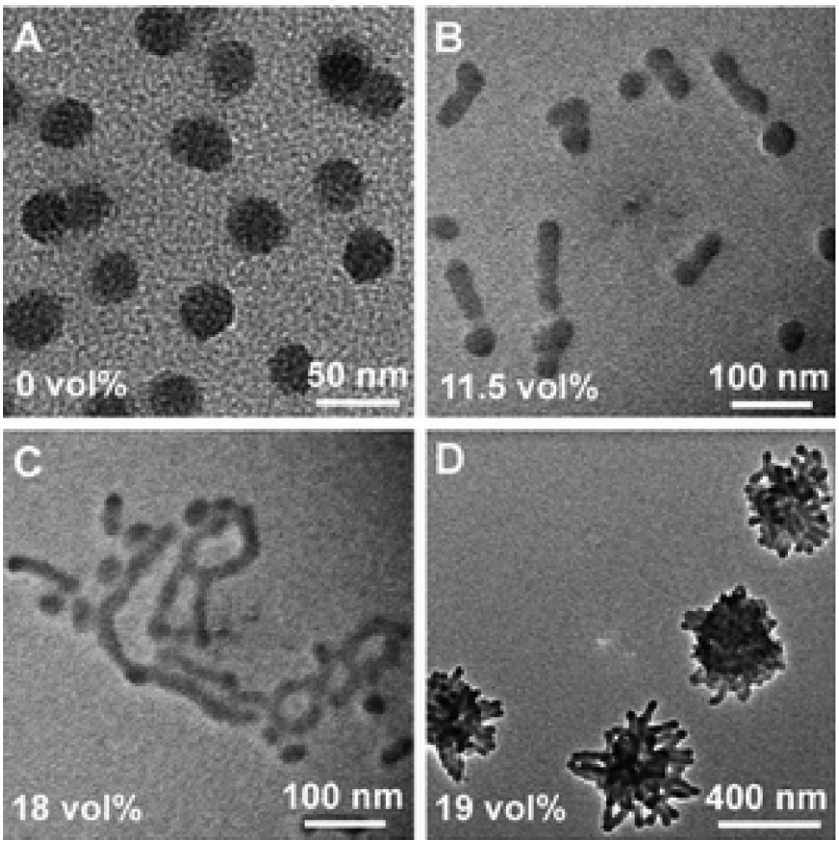

Figure 1. TEM images from samples prepared by casting a solution of copolymer PS_{170} -*b*-PI_{140} in different mixtures of hexane and THF: (A) pure hexane; (B) 11.5 vol.-% of THF; (C) 18 vol.-% of THF; and (D) 19 vol.-% of THF, where samples were prepared under a normal evaporation rate.

samples for the TEM observation were prepared by depositing each PS-*b*-PI copolymer solution on copper grids and let it dry in ambient air at the room temperature. Such observed morphologies are reproducible and can be divided into five categories as a function of the THF content. Namely, (i) when the THF content is less than 10 vol.-%, only spherical micelles with an average size of ≈30 nm are observed in TEM (Figure 1A); (ii) in the range 11–14 THF vol.-%, spherical and cigar-shape micelles coexist (Figure 1B); (iii) when the THF content increases to 15–18 vol.-%, worm-like long cylindrical micelles are clearly visible (Figure 1C); (iv) Further increase of the THF content to 19–22 vol.-% results in a flower-like structure made of twisted long cylindrical micelles (Figure 1D); and (v) finally, as expected, polymeric micelles completely dissolve into individual copolymer chains in the solvent mixture when the THF content reaches ≈22 vol.-% or higher. In general, a thin film made of block copolymer chains confined between the copolymer/substrate and copolymer/air interfaces can undergo both the surface relaxation and reconstruction. The interfacial interaction between a polymer solution and a substrate, such as the wetting/dewetting effect, can also influence the morphology formation on a substrate. Note that in the current study, all the TEM samples are prepared on the copper grid coated with carbon so that the contribution of the interfacial interaction between the solution and substrate remains the same.

It is worth noting that throughout such a morphological transition, the average diameters of spherical and cylindrical micelles remain similar (≈26 nm) in TEM imaging. Initially, we were attracted by such a systematical morphological transition, especially the formation of the flower-like structure in which each loop on its periphery is clearly made of a twisted and folded cylindrical micelle when Figure 1D is enlarged. However, when really thinking about such a change, we found that such a phase transition contradicts our general understanding of the formation of polymeric micelles with different morphologies. Thermodynamically, when a common good solvent is added into a solvent selectively poor for one block, the solubility of that block increases so that the interfacial energy between the soluble and insoluble blocks should decrease. In other words, the soluble blocks should be able to stabilize a larger interface area. The direction of increasing the interface area should follow the change from a lamellar structure to cylindrical micelles and then from cylindrical micelles to spherical micelles; namely, as the THF content increases, we would see the breakdown of long cylindrical micelles into small spherical micelles, not the other way around as shown in Figure 1. Such a contradiction led us to the current study; namely, using a combination of static and dynamic LLS to examine their morphologies in different solvent mixtures in the solution state.

Figure 2 shows that both $\langle R_h \rangle$ and $\langle R_g \rangle$ of the copolymer micelles gradually increase with the THF content when it is below 15 vol.-%. Further increase of the THF content first leads to a sharp increase in both $\langle R_h \rangle$ and $\langle R_g \rangle$ and then followed by an abrupt drop when the THF content reaches ≈22%, revealing the dissolution of each copolymer micelle into individual chains. Note that each LLS measurement was only performed after the copolymer solution reached a steady state that was assessed by monitoring the intensity of the light scattered from the solution as a function of time

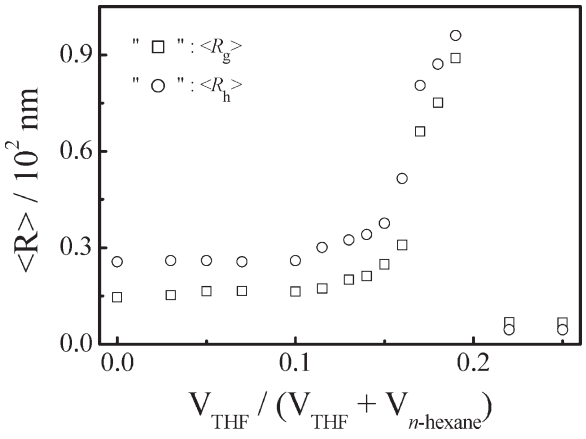

Figure 2. THF content dependent average hydrodynamic radius $\langle R_h \rangle$ and radius of gyration $\langle R_g \rangle$ of diblock copolymer in a mixture of THF and hexane.

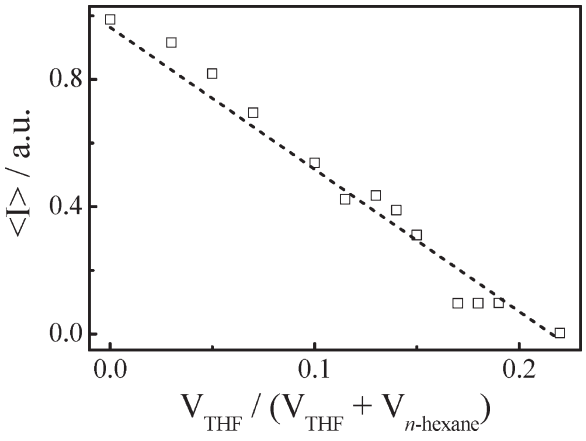

Figure 3. THF content dependent time-averaged scattered light intensity $\langle I \rangle$ of diblock copolymer in a mixture of THF and hexane, where the scattering angle is 20° and the dashed line just guides the eyes.

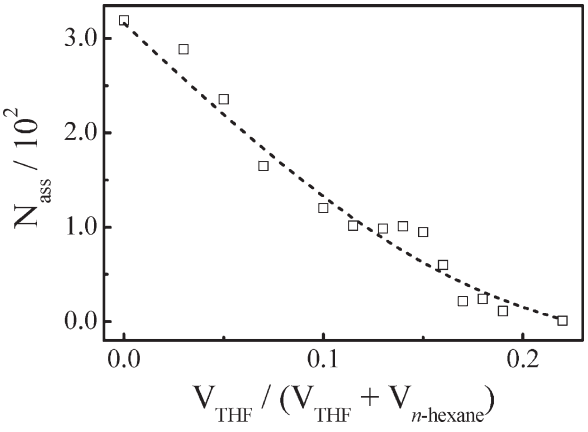

Figure 4. THF content dependent association number (N_{ass}) of diblock copolymer in a mixture of THF and hexane, where the dashed line just guides the eyes.

after the solvent mixing. Surprisingly, the equilibrating process is rather slow even in the solution, typically taking 1–2 months for each copolymer solution to reach its steady state in the solvent mixture. A literature search shows that such a point has been overlooked in the past to some extent. Likely, some of previous studies might be conducted when the copolymer solution mixtures were not in their thermodynamically stable states. Apparently, the results in Figure 2 agree well with those from the TEM measurements; namely, the average size of the scattering subjects, measured in both static and dynamic LLS, presumably polymeric micelles according to the TEM imaging, increases as the THF content increases in the solvent mixture.

However, Figure 3 shows that the time-averaged intensity of the light scattered from the copolymer micelles in the solvent mixture decreases linearly as the THF content increases. Note that in Equation (1), $R_{vv}(q) \approx \langle I \rangle \approx \overline{M}_w$ when $q = 0$ and $C = 0$; and $\overline{M}_w = \Sigma_i n_i M_i^2 / \Sigma_i n_i M_i$, where n_i and M_i are the number and molar mass of the ith scattering subject, respectively. Polymeric micelles are often narrowly dispersed so that $\overline{M}_w \approx M_{chain}\ N_{ass}$, where M_{chain} and N_{ass} are the average molar mass of the chains and the average number of the chains inside each micelle, respectively. For a given copolymer concentration, the decrease of $\langle I \rangle$ can be roughly related to the decrease of N_{ass} since M_{chain} is a constant. After correcting the value of differential refractive index increment (dn/dC) for each solvent mixture and extrapolating $\langle I \rangle$ to $q = 0$, we can convert the THF content dependent $\langle I \rangle_{q=0}$ to its corresponding $\overline{M}_w$ on the basis of Equation (1) and then calculate N_{ass} since $N_{ass} = \overline{M}_w / M_{chain}$.

Figure 4 shows that N_{ass} gradually decreases from ≈320 in pure hexane to ≈30 in 19 vol.-% of THF, and finally becomes one when the THF content reaches ≈22 vol.-%, where we did not

subtract the critical association concentration (CAC) of the coplymer in the solvent mixture when calculating $\overline{M}_w$ because it is extremely low. In principle, the addition of a common good solvent into a selective solvent, in which a diblock copolymer forms spherical micelles, should result in the formation of smaller spherical micelles with a less number of chains inside each micelle if the two solvents are completely mixable because the decrease of the interfacial energy; namely, we would see smaller micelles and a decrease of N_{ass} when the THF content increases in the solvent mixture.

However, Figure 2 shows an opposite trend, i.e., the size increases. On the other hand, the increase of the size of the scattering subjects could be due to the fusion of spherical micelles together to form different morphologies, as shown in Figure 1. In contrast, a comparison of Figure 3 and 4 shows that N_{ass} decreases when $\langle R_g \rangle$ and $\langle R_h \rangle$ increases, clearly revealing that the size increase with the THF content in Figure 2 is not due to formation of cigar-shape or long cylindrical micelles or the flower-like structure in the copolymer solution. The only explanation should be the preferential partition of THF in the PS core because it is an extremely good solvent for PS. To further illustrate possible structures of the chain aggregates in the solution, we calculate the THF content dependent ratio of $\langle R_g \rangle / \langle R_h \rangle$ because it directly reflects the mass distribution of the copolymer chains in space, i.e., the structure of the micelles.

Figure 5 shows that $\langle R_g \rangle / \langle R_h \rangle$ slightly increases in the THF content range 0–15 vol.-%, but around ≈0.6, even smaller than 0.774, predicted for a uniform solid sphere. Such a smaller $\langle R_g \rangle / \langle R_h \rangle$ value is expected for polymeric micelles with a dense core and a relatively loose shell; namely, the loose shell contributes more to $\langle R_h \rangle$ but less to $\langle R_g \rangle$ in comparison with a uniform sphere with an identical radius of $\langle R_h \rangle$. Further increase of the

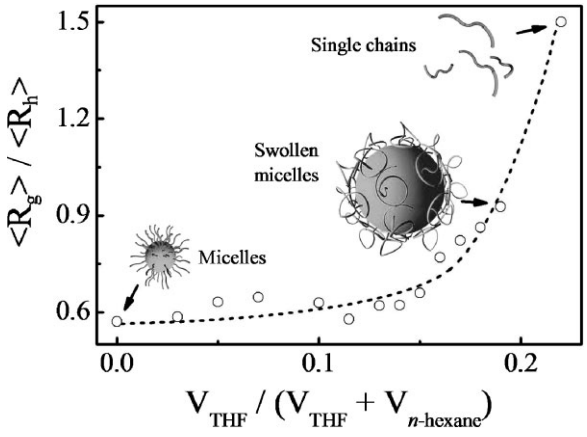

Figure 5. THF content dependence of ratio of average radius of gyration to average hydrodynamic radius $\langle R_g \rangle / \langle R_h \rangle$ of diblock copolymer in a mixture of THF and hexane, where the dashed line just guides the eyes.

THF content in the range 17–19 vol.-% leads to a steep increase of $\langle R_h \rangle$ from ≈35 to ≈90 nm, indicating the swelling of individual copolymer micelles. Meanwhile, $\langle R_g \rangle / \langle R_h \rangle$ increases from 0.7 to 0.9, smaller than 1.0, a value predicted for a hollow sphere with an infinite thin wall. The increase of $\langle R_g \rangle / \langle R_h \rangle$ to ≈0.9 indicates that the PS core of each micelle is highly swollen with THF, as schematically shown in Figure 5. Finally, when the THF content reaches ≈22 vol.-%, both $\langle R_h \rangle$ and $\langle R_g \rangle$ drop to few nanometers (Figure 2) and $\langle R_g \rangle / \langle R_h \rangle$ increases to ≈1.5–1.6, a value predicted for a random coiled chain in good solvent, clearly revealing that the completely dissolution of the micelles.

Further, we can estimate the THF content dependence of the average radius of the micelle core ($\langle R \rangle_{core}$), the shell thickness ($\Delta R_{shell} = \langle R_h \rangle - \langle R \rangle_{core}$) and the average chain density inside each micelle ($\langle \rho \rangle_{micelle} = \overline{M}_w / (4\pi \langle R_h \rangle^3 N_A / 3)$) by combining static and dynamic LLS results together. Previously, after assuming that a core-shell micelle has a uniform core and shell with different chain densities, we were able to estimate $\langle R \rangle_{core}$ from its $\langle R_g \rangle / \langle R_h \rangle$.[33]

Figure 6 shows that initially, the shell and the core have a similar size, but $\langle R \rangle_{core}$ increases while ΔR_{shell} slightly decreases as the THF content increases in the range 0–10 vol.-%.

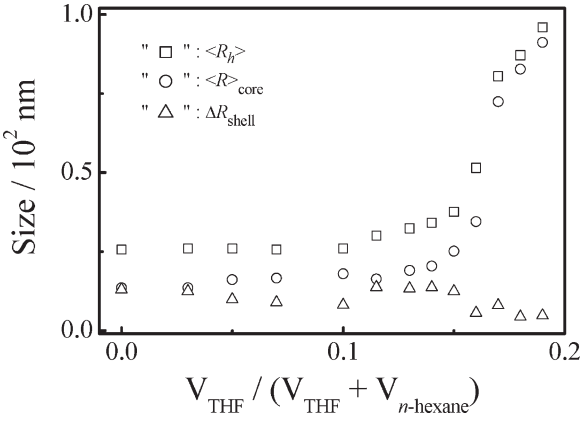

Figure 6. THF content dependence of average radius of the core ($\langle R \rangle_{core}$) and shell thickness (ΔR_{shell}) of spherical micelles in a mixture of THF and hexane, where we re-plot $\langle R_h \rangle$ just for comparison, especially in the highly swollen state (19 vol.-% of THF).

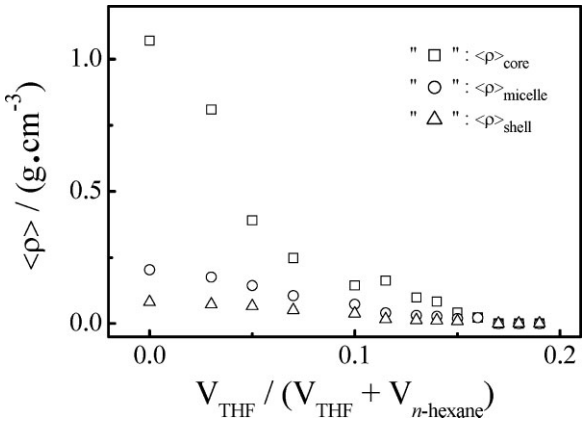

Figure 7. Variations of the average densities of the spherical micelle ($\langle\rho\rangle_{micelle}$), its core ($\langle\rho\rangle_{core}$) and shell ($\langle\rho\rangle_{shell}$) as a function of the THF content.

Further increase of the THF content leads to a much high degree of swelling of the core. The results in Figure 6 directly reveal that THF swells the PS core, presumably due to the preferential partition of THF inside the PS block, and the slight contraction of the stretched PI blocks in the shell when the core is small. A combination of Figure 2, 4 and 6, i.e., $\langle R\rangle_{core}$, ΔR_{shell} and N_{ass}, enables us to estimate the chain densities of the core and the shell ($\langle\rho\rangle_{core}$ and $\langle\rho\rangle_{shell}$), respectively from $M_{PS}\ N_{ass}/(4\pi\ \langle R_{core}\rangle^3 N_A/3)$ and $M_{PI}\ N_{ass}/[4\pi(\langle R_h\rangle^3 - \langle R\rangle^3_{core})N_A/3]$. Figure 7 shows a large decrease of $\langle\rho\rangle_{core}$ as the THF content increases, further indicating that the core is gradually swollen and become less dense due to the preferential partition of THF in the core. Figure 7 also shows that $\langle\rho\rangle_{shell}$ decreases in the same THF range. This is because the increase of the THF content leads to the decrease of N_{ass} and the increase of $\langle R_h\rangle$, but ΔR_{shell} nearly remains.

The above LLS results unambiguously demonstrate an expected PS-core-swelling process as a common good solvent (THF) is mixed with hexane (a solvent selectively poor for PS). During the swelling process, the morphology of the diblock copolymer micelles remains spherical. There is no surprising from the thermodynamic point of view. As the quality of the solvent mixture becomes better for the PS block, the interfacial energy between the PS core and PI shell reduces. As a result, the given amount of the PI blocks can stabilize a larger interfacial area, resulted from the preferential partition of THF in the PS core. The apparent disagreement between the TEM and LLS results leads us to conclude that those non-spherical morphologies must be formed during the TEM sample preparation. Actually, the control of the solvent evaporation was utilized to alternate the micelle morphology and the orientation and lateral ordering of the domains made of block copolymers.[34–39]

In order to test such an effect of the solvent evaporation rate, we purposely prepared the TEM samples in three different ways when the THF content is in the range 11 to 22 vol.-%; namely, (1) very quick evaporation in air by drying each sample with a hair dryer; (2) normal evaporation in ambient air at the room temperature; and (3) very slow evaporation in the saturated vapor of the solvent mixture. The procedures have been detailed in the Section of the TEM sample preparation.

Figure 8 show that when the THF content is 11.5, 14, and 16 vol.-%, the copolymer samples prepared with the normal evaporation rate show both spherical and cylindrical micelles (Figure 8B, E, and H), while for higher THF contents, long cylindrical micelles are clearly formed. The cylindrical micelles in these samples have an average diameter of ≈26 nm.

The effect of the evaporation rate is obvious, resulting in dramatically different micelle morphologies. As expected, the very quick evaporation rate enables us to frozen and capture spherical morphology of the micelles in the solutions with an average diameter of ≈25 nm, especially when the THF content is relatively low (Figure 8A). This is because individual micelles in the solution have no sufficient time to fuse together. In the presence of more THF, the copolymer chains are more mobile inside each spherical micelle in the solution so that it is easier for them to fuse together to form cigar-shape micelles. This is why for the samples prepared with 14 and 16 vol.-% THF, spherical micelles are dominant but a small amount of fused micelles are also observable (Figure 8D and G). Note that a considerable fraction of the spherical micelles are larger, presumably due to the fusion of several smaller ones together. On the other hand, the very slow evaporation results in the morphologies which are more close to the thermodynamically stable state in the copolymer melt; namely, long cylindrical micelles and even lamellar structure (Figure 8C, F, and I). The cylindrical micelles or the lamellar structure in these samples have a slightly smaller average diameter or layer space of ≈22 nm, which is reasonable because a cylindrical micelle has a less space-filling problem than a spherical one for a given diblock copolymer.

A comparison of the results of LLS and TEM, obtained with different evaporation rates, clearly shows that there are only spherical micelles in the copolymer solutions, which agrees with the reported phase diagram.[40] The cylindrical micelles and the flower-like structure (Figure 1) are formed during the drying process in the TEM sample preparation,

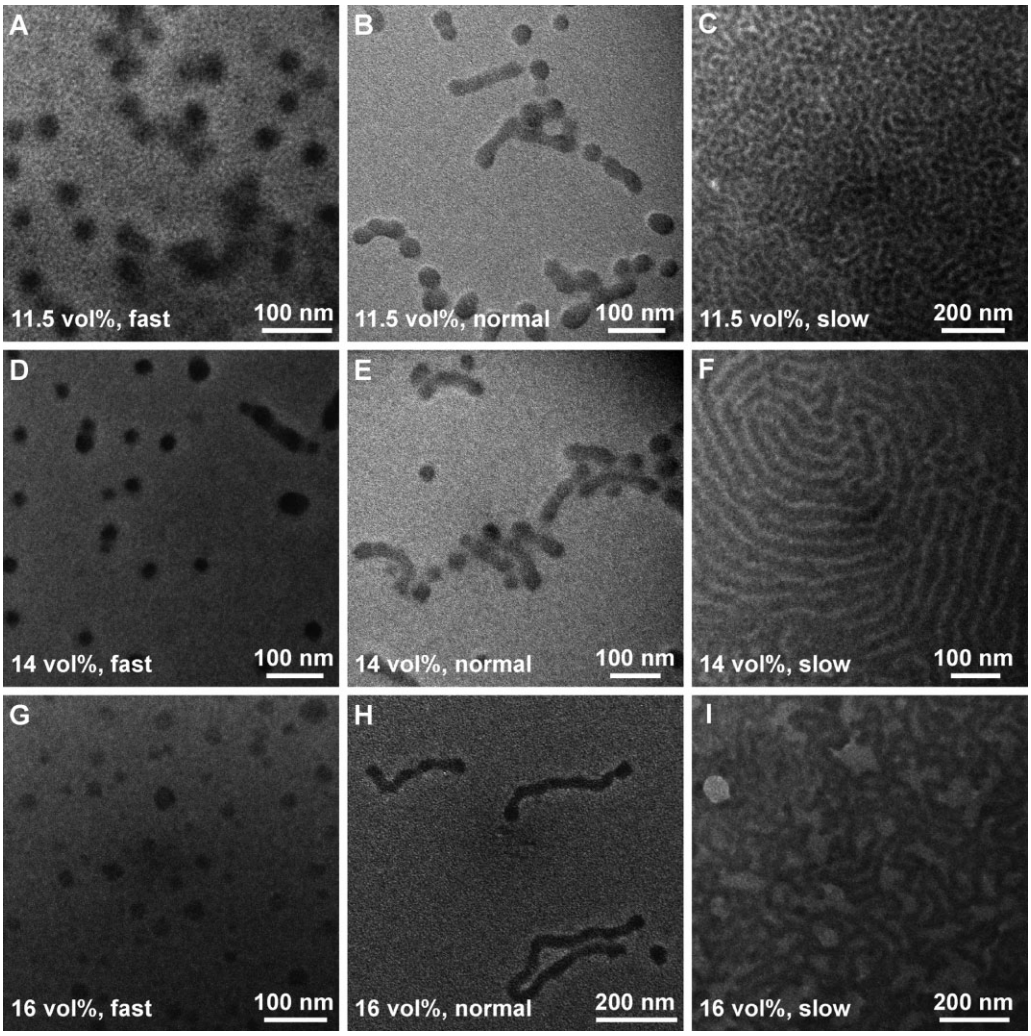

Figure 8. TEM images of micelle samples obtained from the solution containing 11.5, 14, and 16 vol.-% THF under different solvent evaporation rates, respectively.

which involves two important processes;[41,42] namely, the evaporation of solvent and the fusion of small spherical micelles. The boiling points of THF and hexane are 66 and 69 °C, respectively. After the copolymer solution is deposited on the copper grid, the two solvents start to evaporate with a similar rate.

The solvent evaporation is characterized by the evaporation time constant (τ_e), which can be controlled by the drying condition. The fusion of two spherical micelles together is governed by two characteristic times; namely, the interaction time (τ_i) and the fusion time (τ_f). τ_i is related to the diffusion time and the inter/micelle interaction distance; while τ_f mainly depends on the mobility (relaxation) of the chains in each micelle. When $\tau_i \ll \tau_f$, each micelle behaves like a tiny glass ball so that the fusion is kinetically frozen and the micelles are stabilized by the viscoelastic effect.[43–47] During the solvent evaporation, small spherical micelles are pushed together so that τ_i increases. The addition of a common good solvent looses the core and increases the solubility of the PS blocks inside so that τ_f decreases. This explains why small spherical micelles are fused together to form structures with different morphologies when THF is added in the copolymer solution. On the other hand, if $\tau_f \gg \tau_e$, spherical micelles formed in the solution are frozen during the TEM sample preparation.

Practically, in order to obtain a true morphology of polymeric micelles/aggregates in dispersion, one should use a´cryo-TEM or a combination of freeze drying of a solution and a normal room-temperature TEM. Namely, (i) placing a TEM copper grid on the bottom of a glass cell; (ii) transfer a small amount (250 μL or less) of polymer solution into the cell to make sure that the grid is completely immerged in the solution; (iii) inserting the glass cell into liquid nitrogen to quickly freeze the solution into a solid; (iv) transferring the solution in its

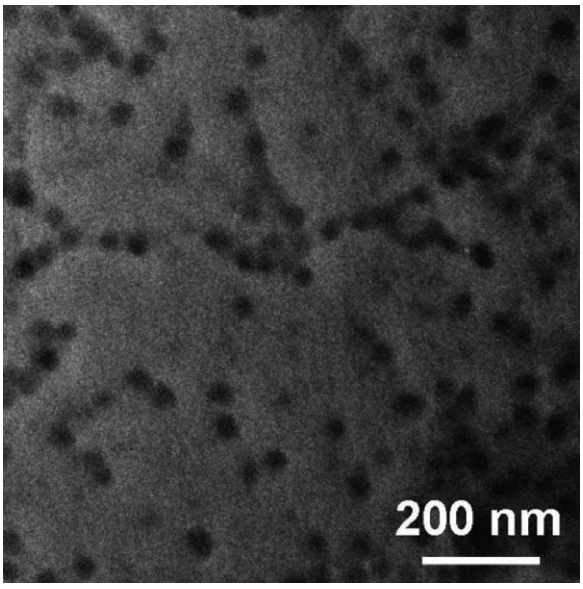

Figure 9. TEM image of a micelle sample prepared by freeze drying of a solution of copolymer in a mixture of hexane and THF (16 vol.-%).

frozen solid state into a freeze-drying device; (v) removing solvent directly from its solid state to its vapor state without melting; and (vi) imaging its morphology in a normal TEM at the room temperature after the solvent is completely removed. By following the above procedure, we were able to obtain the true spherical morphology of the polymeric micelles in the solvent mixture (16 vol.-% THF), as shown in Figure 9, without any visible cylindrical micelles. Figure 10 schematically summarizes our discussion about how diblock PS-*b*-PI micelles with different morphologies are formed in the solvent mixture and in the TEM sample preparation with different solvent evaporation rates.

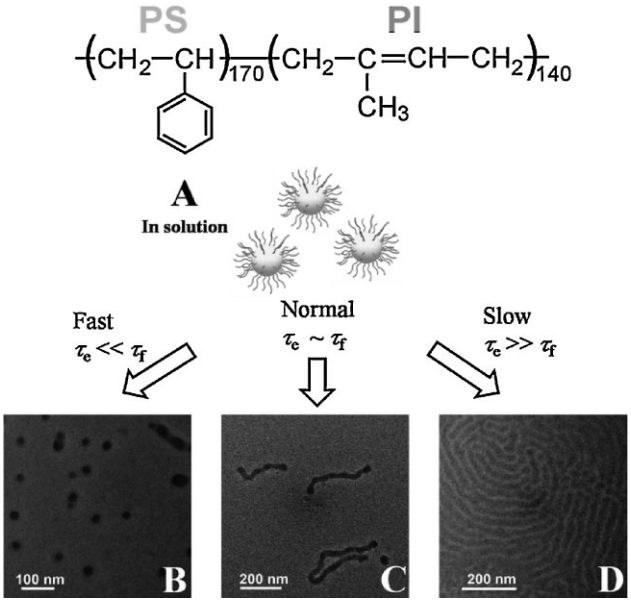

Figure 10. Schematic of solvent evaporation rate-induced morphological transition of diblock PS-*b*-PI micelles in a mixture of THF and hexane: (A) Spherical; (B) partially fused spherical micelles; (C) formation of cylindrical micelles; and (D) formation of long cylindrical micelles or lamellar structures.

Conclusion

A comparative study of the micelle formation of poly(styrene-*b*-isoprene) (PS_{170} -*b*-PI_{140}) diblock copolymer in different binary solvent mixtures of THF and hexane by LLS and the morphologies observed in TEM reveals that there are only spherical micelles in the solution. The addition of a common good solvent (THF) gradually swells the PS core so that the size of the micelles increases, and at the same time, gradually dissolves the micelles so that the average number of the chains inside each micelle decreases. The cigar-sharp and long cylindrical micelles as well as the exotic flower-like structure observed in TEM at the room temperature are simply formed during the solvent evaporation process in the TEM sample preparation. The formation of different morphologies is governed by the solvent evaporation rate and the micelle fusion and interaction times. Our current results clearly demonstrate that it is really necessary and vitally important to combine different methods, instead of using only a normal TEM to characterize the morphologies of block copolymer micelles in solution, especially when computer simulations are compared with the morphologies generated from a copolymer solution. Fairly speaking, more and more people are realizing that it is really necessary to use cryo-TEM to characterize different morphologies formed in polymer solutions. However, there still lack sufficient attention in this aspect, partially due to the fact that most of researchers are not able to access cryo-TEM at this moment, especially when organic solvents are used. Our current study serves as a further alarm to those who are interested in morphologies of block copolymers in solutions. We have demonstrated that, instead of

cryo-TEM, one could use the freeze-drying method described in this paper to prepare TEM samples, which can lead to a better description of morphologies in solutions if it is done properly. It should be noted that the kinetic effect discussed here is not completely evil because we can play it to obtain some desired morphologies or nanostructures for various potential applications.

Acknowledgements: Financial support from the *National Natural Scientific Foundation of China* (NNSFC, Projects 50773077 and 20934005) and the *Hong Kong Special Administration Region Earmarked* (RGC, Projects CUHK4037/07P, 2160331; CUHK4046/08P, 2160365; CUHK4039/08P, 2160361; and CUHK4042/09P, 2160396) is gratefully acknowledged.

Received: November 9, 2010; Revised: December 27, 2010; Published online: February 14, 2011; DOI: 10.1002/macp.201000696

Keywords: block copolymers; laser light scattering; polymer morphology; PS-*b*-PI; TEM

[1] O. Benny, O. Fainaru, A. Adini, F. Cassiola, L. Bazinet, I. Adini, E. Pravda, Y. Nahmias, S. Koirala, G. Corfas, R. J. D'Amato, J. Folkman, *Nat. Biotechnol.* **2008**, *26*, 799.
[2] J. A. MacKay, M. N. Chen, J. R. McDaniel, W. G. Liu, A. J. Simnick, A. Chilkoti, *Nat. Mater.* **2009**, *8*, 993.
[3] H. Wang, W. J. Lin, K. P. Fritz, G. D. Scholes, M. A. Winnik, I. Manners, *J. Am. Chem. Soc.* **2007**, *129*, 12924.
[4] H. Wang, X. S. Wang, M. A. Winnik, I. Manners, *J. Am. Chem. Soc.* **2008**, *130*, 12921.
[5] X. H. Yan, F. T. Liu, Z. Li, G. J. Liu, *Macromolecules* **2001**, *34*, 9112.
[6] S. Jain, F. S. Bates, *Science* **2003**, *300*, 460.
[7] E. B. Zhulina, M. Adam, I. LaRue, S. S. Sheiko, M. Rubinstein, *Macromolecules* **2005**, *38*, 5330.
[8] J. Bang, S. Jain, Z. B. Li, T. P. Lodge, J. S. Pedersen, E. Kesselman, Y. Talmon, *Macromolecules* **2006**, *39*, 1199.
[9] T. Smart, H. Lomas, M. Massignani, M. V. Flores-Merino, L. R. Perez, G. Battaglia, *Nano Today* **2008**, *3*, 38.
[10] A. Halperin, M. Tirrell, T. P. Lodge, *Adv. Polym. Sci.* **1992**, *100*, 31.
[11] E. Minatti, P. Viville, R. Borsali, M. Schappacher, A. Deffieux, R. Lazzaroni, *Macromolecules* **2003**, *36*, 4125.
[12] N. Ouarti, P. Viville, R. Lazzaroni, E. Minatti, M. Schappacher, A. Deffieux, R. Borsali, *Langmuir* **2005**, *21*, 1180.
[13] L. F. Zhang, A. Eisenberg, *Science* **1995**, *268*, 1728.
[14] L. F. Zhang, A. Eisenberg, *J. Am. Chem. Soc.* **1996**, *118*, 3168.
[15] L. F. Zhang, A. Eisenberg, *Macromolecules* **1999**, *32*, 2239.
[16] Y. S. Yu, L. F. Zhang, A. Eisenberg, *Macromolecules* **1998**, *31*, 1144.
[17] H. Y. Huang, R. Hoogenboom, M. A. M. Leenen, P. Guillet, A. M. Jonas, U. S. Schubert, J. F. Gohy, *J. Am. Chem. Soc.* **2006**, *128*, 3784.
[18] I. LaRue, M. Adam, M. Pitsikalis, N. Hadjichristidis, M. Rubinstein, S. S. Sheiko, *Macromolecules* **2006**, *39*, 309.
[19] P. Bhargava, Y. F. Tu, J. X. Zheng, H. M. Xiong, R. P. Quirk, S. Z. D. Cheng, *J. Am. Chem. Soc.* **2007**, *129*, 1113.
[20] K. Iyama, T. Nose, *Macromolecules* **1998**, *31*, 7356.
[21] Y. Y. Won, A. K. Brannan, H. T. Davis, F. S. Bates, *J. Phys. Chem. B* **2002**, *106*, 3354.
[22] H. W. Shen, L. F. Zhang, A. Eisenberg, *J. Am. Chem. Soc.* **1999**, *121*, 2728.
[23] Q. J. Chen, H. Zhao, T. Ming, J. F. Wang, C. Wu, *J. Am. Chem. Soc.* **2009**, *131*, 16650.
[24] F. Sterpone, G. Briganti, S. Melchionna, C. Pierleoni, *Langmuir* **2008**, *24*, 6067.
[25] Y. Talmon, *J. Colloid Interfaces Sci.* **1983**, *93*, 366.
[26] T. Xu, Y. Q. Zhu, S. P. Gido, T. P. Russell, *Macromolecules* **2004**, *37*, 2625.
[27] K. Schmidt, H. G. Schoberth, M. Ruppel, H. Zettl, H. Hänsel, T. M. Weiss, V. Urban, G. Krausch, A. Böker, *Nat. Mater.* **2008**, *7*, 142.
[28] C. Osuji, P. J. Ferreira, G. P. Mao, C. K. Ober, J. B. Vander Sande, E. L. Thomas, *Macromolecules* **2004**, *37*, 9903.
[29] M. M. Mok, S. Pujari, W. R. Burghardt, C. M. Dettmer, S. T. Nguyen, C. J. Ellison, J. M. Torkelson, *Macromolecules* **2008**, *41*, 5818.
[30] D. E. Angelescu, J. H. Waller, D. H. Adamson, R. A. Register, P. M. Chaikin, *Adv. Mater.* **2007**, *19*, 2687.
[31] S. H. Kim, M. J. Misner, T. Xu, M. Kimura, T. P. Russell, *Adv. Mater.* **2004**, *16*, 226.
[32] L. Z. Hong, F. Jin, J. F. Li, Y. J. Lu, C. Wu, *Macromolecules* **2008**, *41*, 8220.
[33] Y. F. Tu, X. H. Wan, D. Zhang, Q. F. Zhou, C. Wu, *J. Am. Chem. Soc.* **2000**, *122*, 10201.
[34] S. H. Kim, M. J. Misner, T. Xu, M. Kimura, T. P. Russell, *Adv. Mater.* **2004**, *16*, 226.
[35] G. Kim, M. Libera, *Macromolecules* **1998**, *31*, 2569.
[36] G. Kim, M. Libera, *Macromolecules* **1998**, *31*, 2670.
[37] K. Fukunaga, H. Elbs, R. Magerle, G. Krausch, *Macromolecules* **2000**, *33*, 947.
[38] K. Fukunaga, T. Hashimoto, H. Elbs, G. Krausch, *Macromolecules* **2002**, *35*, 4406.
[39] A. Turturro, E. Gattiglia, P. Vacca, G. T. Viola, *Polymer* **1995**, *36*, 3987.
[40] A. K. Khandpur, S. Förster, F. S. Bates, I. W. Hamley, A. J. Ryan, W. Bras, K. Almdal, K. Mortensen, *Macromolecules* **1995**, *28*, 8796.
[41] H. G. Cui, Z. Y. Chen, K. L. Wooley, D. J. Pochan, *Macromolecules* **2006**, *39*, 6599.
[42] H. G. Cui, Z. Y. Chen, S. Zhong, K. L. Wooley, D. J. Pochan, *Science* **2007**, *317*, 647.
[43] M. H. Siu, H. Y. Liu, X. X. Zhu, C. Wu, *Macromolecules* **2003**, *36*, 2103.
[44] M. H. Siu, C. He, C. Wu, *Macromolecules* **2003**, *36*, 6588.
[45] C. Wu, W. Li, X. X. Zhu, *Macromolecules* **2004**, *37*, 4989.
[46] H. W. Chen, Q. J. Zhang, J. F. Li, Y. W. Ding, G. Z. Zhang, C. Wu, *Macromolecules* **2005**, *38*, 8045.
[47] G. Z. Zhang, C. Wu, *Adv. Polym. Sci.* **2006**, *195*, 101.